SAND2022-9805C

Effects of non-thermal reactivity on wedge-induced oblique detonation waves

Swapnil Desai[1], Yujie Tao[2], Raghu Sivaramakrishnan[3], Jacqueline H. Chen[1]

[1]Sandia National Laboratories, USA, [2]Southeast University, China, [3]Argonne National Laboratory, USA

Background-Objective

The Oblique Detonation Wave Engine (ODWE) is among the promising choices for hypersonic propulsion systems. An understanding of the ignition, propagation, and stability of an oblique detonation wave (ODW) is critical to harnessing its propulsive potential. In such high speed reacting flows, there is a high probability of occurrence of non-thermal reactions due to the presence of non-trivial amounts of highly reactive radicals including H, O and OH apart from O_2 as demonstrated recently [M. P. Burke, S. J. Klippenstein, Nat. Chem. 9 (2017) 1078 - 1082, Y. Tao, A. W. Jasper, Y. Georgievskii, S. J. Klippenstein, R. Sivaramakrishnan, Proc. Combust. Inst. 38 (2021) 515–522]. In combustion simulations, a typical 3-body reaction H + OH (+ M) → H_2O (+ M) is a simplified description of a 2 step process: R1: H + OH → H_2O*, R2: H_2O* + M → H_2O + M, where the short-lived H_2O* is always assumed to be under thermal equilibrium while M typically assumed to be a chemically inert "bath gas" molecule

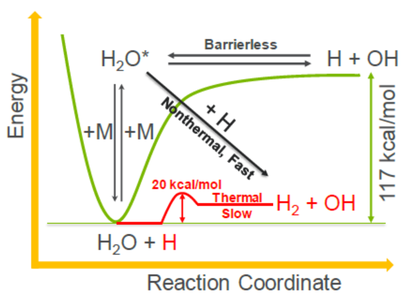

Figure 1. Schematic potential energy surface of the thermal and non-thermal reactions in the recombination reaction H + OH (+M) → H2O + M (Adopted from Tao et al. Proc. Combust. Inst. 38 (2021) 515–522)

However, non-trivial mole fractions of reactive radicals (H, O, OH) and O_2 are usually present in practical flames. As shown in the figure above, the thermal reaction of H_2O with H has a pronounced barrier of 20 kcal/mol whereas non-thermal reaction of H_2O* with H can proceed much faster. Hence, the probability of non-thermal reactivity is higher under such conditions. The objective of the present work is to understand the initiation and structure of ODW in stoichiometric H_2-air mixtures through high-order numerical simulations on a two-dimensional adaptive grid including non-thermal reactivity.

Inclusion of non-thermal reactivity in macroscopic kinetic model

7 additional reactions were added to the base H_2/air chemical model by Miller et al. (Prog. Energ. Combust., 83 (2021), 10886) consisting of 26 reactions to represent non-thermal reactivity as described by Tao et al. (Proc. Combust. Inst. 38 (2021) 515–522) and Burke et al. (Nat. Chem., 9, (2017), 1078-1082)

Here, AB* is the rovibrationally excited species that can form due to the radical/radical recombination reaction R5 or the radical/molecule association reaction R16, while X is its collision partner which can either be a radical such as H, O, OH or a molecule such as O_2. Inclusion of these additional non-thermal termolecular reactions has been observed to cause a reduction in global reactivity due to: 1) reduction in overall radical branching ratio, and 2) reduction in radical mole fractions. In the present study, appropriate correction factors were also applied to the rate constants of the respective recombination and association reactions: R5 and R16 to account for their reduced fluxes due to the inclusion of such non-thermal termolecular reactions.

Numerical Methods, Computational Configuration and Initial Conditions

The fully compressible governing equations for reacting flows: Navier-Stokes, continuity, species and energy equations were solved using the exascale ready code Pele-C (https://amrex-combustion.github.io/PeleC) with:

- 2nd order finite volume approach for spatial discretization
- 7th order WENO-Z scheme for convective fluxes
- Time advance based on spectral deferred correction approach
- 3 AMR Levels: $\Delta_{x,max} = 12.5\ \mu m, \Delta_{x,min} = 1.5625\ \mu m$

Based on the finest grid resolution, y+ was found to be between 0.2 and 18 along the wedge surface at steady state conditions. Hence, the simulations in the present study are implicit Large Eddy Simulations (iLES). Three different 2D unsteady iLES cases – 1) Baseline, 2) Termolecular and 3) Corrected Termolecular with correction factors applied to rate constants of R5 and R16 were performed. The hypersonic vehicle was assumed to be traveling at a height of 15 km and a speed of Mach 10. iLES was performed for the combustor region as represented by the rectangular domain highlighted by the dotted lines in Figure 2. The coordinates of the computational domain were rotated to align with the direction along the wedge surface such that the resulting wedge angle is 19°. Due to the specific design of the vehicle, the incoming fuel/air mixture typically undergoes compression twice via two equally strong oblique shocks before entering the combustor.

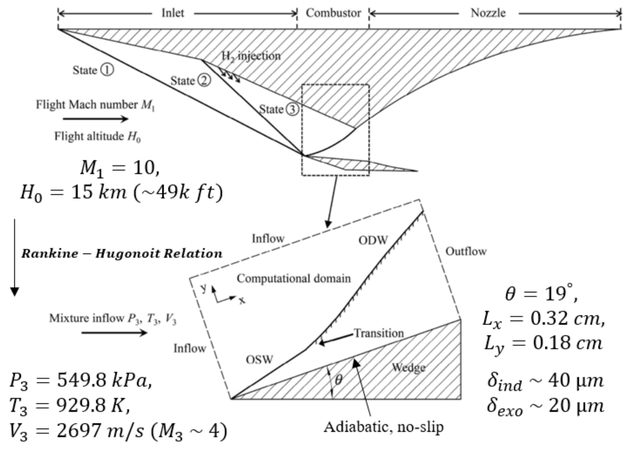

Figure 2. Schematics of an ODW-based and the wedge-induced ODW computational domain (Adopted from Teng et al. J. Flu. Mech. 913 (2020) A1)

Hence, based on the chosen flight altitude and Mach number, the mixture inflow parameters were determined based on the Rankine-Hugoniot relation as listed in Fig. 2. As such, each iLES case was initialized with a stoichiometric H_2/ air in the entire domain at pressure P_3 and temperature T_3. The inflow conditions were fixed at the free stream values. In this study, we utilized a modified version of the 9 species H_2/air chemical model by Miller et al. (Prog. Energy Combust., 83 (2021), 10886) which includes 7 non-thermal termolecular reactions in addition to the 27 baseline reactions. The additional termolecular reactions were only invoked in the second and third cases.

Determination of Correction Factors

The inclusion of non-thermal termolecular reactions also leads to a reduction in the reaction fluxes of the incipient recombination/association reactions R5 and R16. To account for this, appropriate correction factors were applied to the rate constants of the respective incipient reactions based on the procedure described in Tao et al. (Proc. Combust. Inst. 38 (2021) 515–522).

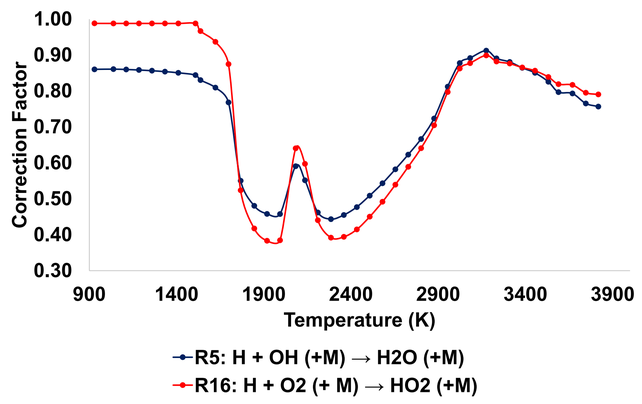

Figure 3. Computed correction factors with respect to temperature for reactions R5 and R16

Figure 3 depicts the correction factors computed as a function of temperature for the two incipient reactions R5 and R16. It can be seen that the magnitude of correction factor exhibits a nonmonotonic behavior with respect to temperature. A correction factor close to unity indicates that reactions R5 and R16 proceed at their normal/baseline rates whereas a correction factor smaller than unity indicates a reduction in the rates of progress of R5 and R16, respectively.

Results

Influence of non-thermal reactivity on ODW initiation length

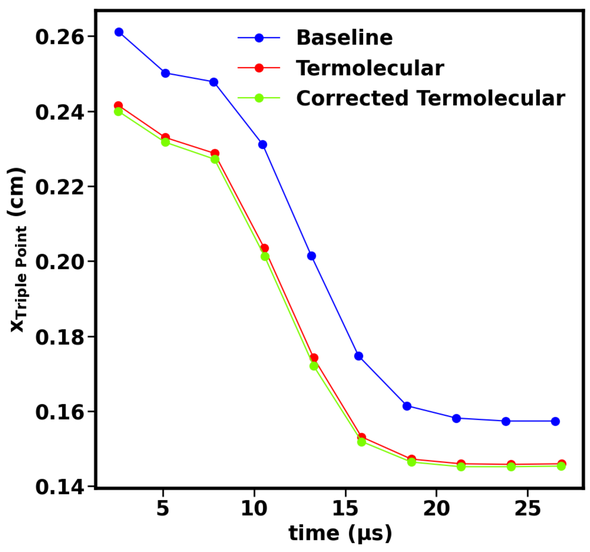

Figure 4. Temporal evolution of the triple point (peak heat release rate) location

The temporal evolution of the triple point (peak heat release rate) location from the left boundary and parallel to the wedge surface was monitored to determine the ODW initiation length. As shown in Figure 4, the triple point is found to be the farthest in the baseline case (0.261 cm) compared to either the termolecular (0.242 cm) or corrected termolecular cases (0.24 cm) during the initial stages. As time progresses, the ODW in each case enters the unsteady propagation stage where the triple point moves closer to the left boundary before eventually stabilizing at a specific location where the propagation velocity of the oblique detonation wave matches the inflow velocity. At the steady state, the triple point is closer to the left boundary in the termolecular (0.146 cm) and corrected termolecular (0.145 cm) cases than in the baseline case (0.157 cm). This translates to over 7% reduction in ODW initiation length. Correcting the rate constants of reactions R5 and R16, however, appears to have a negligible effect on the ODW initiation length.

Influence of non-thermal reactivity on ODW cellular instabilities

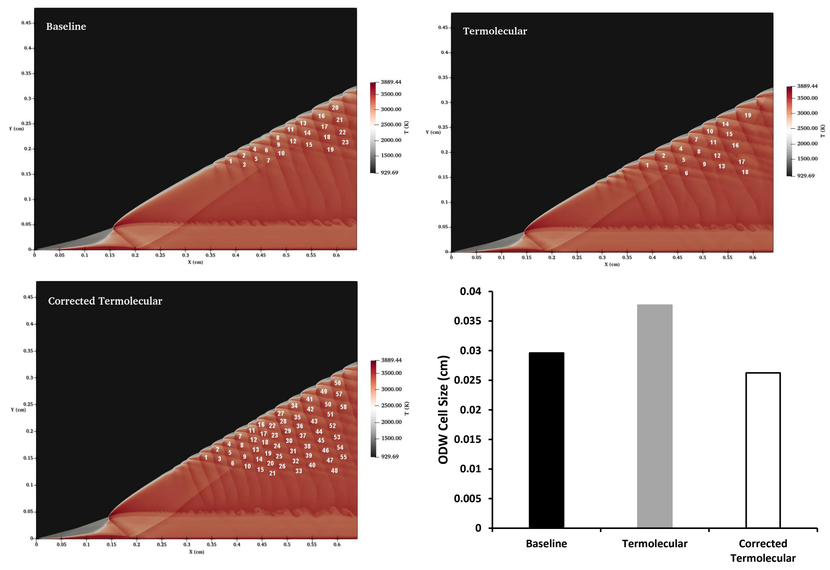

Figure 5. Steady state temperature field in the baseline (top left), termolecular (top right) and corrected termolecular (bottom left) cases. Numbers overlapping the temperature field denote the ODW cells that were utilized to quantify the ODW cell-size in each case.

Top left, top right and bottom left subplots in Figure 5 denote the temperature field at the steady state in each of the cases. The numbers overlapping the temperature field denote the ODW cells that were identified to quantify the ODW cell-size in each case. The bottom right figure in Figure 5 represents the average ODW cell-size that was measured in each case. In the present study, the cell size was identified as the distance between consecutive triple points in the direction parallel to the ODW. Inclusion of non-thermal reactivity alone increases the ODW cell-size by over 27% in relation to the baseline case. On the other hand, applying correction factors on top of including non-thermal termolecular reactions leads to a reduction in ODW cell-size by more than 11% with respect to the baseline case. Analogous to the shortening of the ODW initiation length, the spatial location of onset of cellular instabilities also shifts upstream in the termolecular and corrected termolecular cases.

Influence of non-thermal reactivity on steady ODW structure

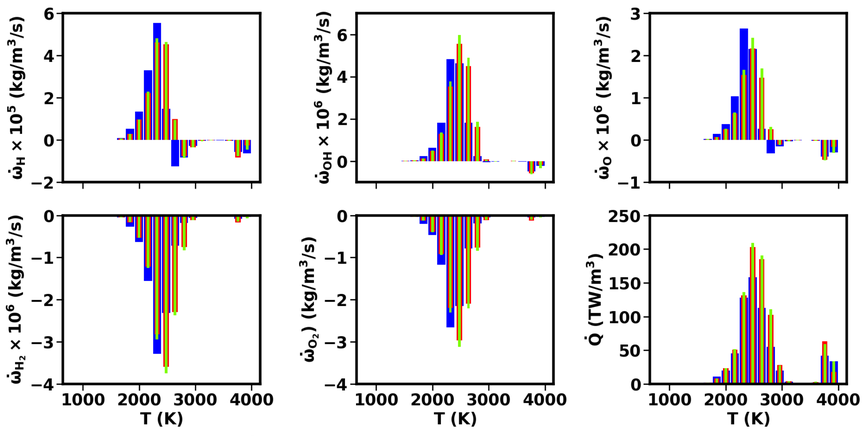

Figure 6. Mean reaction rates of key species and heat release rate conditioned on temperature at the steady state in the Baseline (blue bars), Termolecular (red bars) and Corrected Termolecular (green bars) cases.

The mean reaction rates of key species conditioned on temperature are shown in Figure 6 for each of the cases. It can be seen that the peak reaction rate of radicals, H_2 and O_2 in the termolecular (blue bars) and corrected termolecular (green bars) cases are lower than the baseline (red bars) case when T < 2300 K. An opposite trend is observed when T > 2300 K wherein the mean reaction rates of key species are noticeably higher in the termolecular and corrected termolecular cases. Consequently, the peak heat release rate is also significantly higher in the presence of non-thermal reactivity, especially at higher temperatures, i.e. T > 2300 K.

Dominant reactions contributing to mean heat release rate

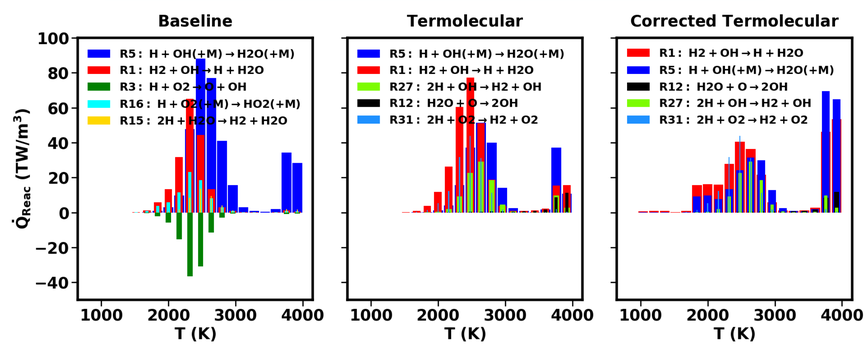

Figure 7. Heat of reaction of 5 most dominant reactions contributing to mean heat release rate conditioned on temperature in each case.

The heat of reaction of the 5 most dominant reactions contributing to mean heat release rate conditioned on temperature is presented in Figure 7 for each case. It can be seen that reactions R5 and R1 contribute the most to mean exothermicity in all the cases. While the endothermic reaction R3 is observed to be dominant in the baseline case, it is replaced by the exothermic reaction R12 in the termolecular and corrected termolecular cases. Meanwhile, the two termolecular reactions R27 and R31, that provide additional H_2 and O_2 along with the OH radical within the reaction zone, are found to be among the most dominant reactions contributing to mean exothermicity in the termolecular and corrected termolecular cases.

Conclusion

The present study shows that non-thermal reactivity can lead to noticeable reduction in induction length and a simultaneous increase in instantaneous heat release rate associated with ODW under ODWE relevant conditions. Inclusion of non-thermal reactivity can also affect the onset location as well as the size of cellular instabilities of the ODW. Therefore, it is important to properly account for non-thermal reactions in high speed reacting flows.

Acknowledgements: The work at Sandia was supported by the US Department of Energy, Office of Basic Energy Sciences, Division of Chemical Sciences, Geosciences, and Biosciences as well as by the Exascale Computing Project (17-SC-20-SC), a collaborative effort of the U.S. Department of Energy Office of Science and the National Nuclear Security Administration. Sandia National Laboratories is a multi-mission laboratory managed and operated by National Technology and Engineering Solutions of Sandia, LLC., a wholly owned subsidiary of Honeywell International, Inc., for the U.S. Department of Energy's National Nuclear Security Administration under contract DE-NA- 0003525 The work at Argonne National Laboratories was supported by the U.S. Department of Energy, Office of Science, Office of Basic Energy Sciences, Division of Chemical Sciences, Geosciences, and Biosciences under Contract DE-AC02-06CH11357. Support for R. S. and Y. T. was provided as part of the Argonne-Sandia Consortium on High-Pressure Combustion Chemistry (ANL FWP 59[illegible]). Y. T. acknowledges the financial support from the National Natural Science Foundation of Jiangsu Province (Grant No. BK20210236).